MOLECULAR AND CELLULAR BIOLOGY, Mar. 2005, p. 2191–2199 Vol. 25, No. 6
0270-7306/05/$08.00+0 doi:10.1128/MCB.25.6.2191–2199.2005

Congenital Semilunar Valvulogenesis Defect in Mice Deficient in Phospholipase Cε†

Makoto Tadano,[1]‡ Hironori Edamatsu,[1]‡ Susumu Minamisawa,[2] Utako Yokoyama,[2] Yoshihiro Ishikawa,[2] Noboru Suzuki,[3] Hiromitsu Saito,[3] Dongmei Wu,[1] Misa Masago-Toda,[1] Yuriko Yamawaki-Kataoka,[1] Tomiyoshi Setsu,[4] Toshio Terashima,[4] Sakan Maeda,[5] Takaya Satoh,[1] and Tohru Kataoka[1]*

Division of Molecular Biology, Department of Molecular and Cellular Biology,[1] Division of Developmental Neurobiology, Department of Brain Sciences,[4] and Division of Molecular Pathology, Department of Biomedical Informatics,[5] Kobe University Graduate School of Medicine, Chuo-ku, Kobe, Department of Physiology, Yokohama City University School of Medicine, Kanazawa-ku, Yokohama,[2] and Department of Animal Genomics, Functional Genomics Institute, Mie University Life Science Research Center, Tsu-shi, Mie,[3] Japan

Received 1 September 2004/Returned for modification 18 October 2004/Accepted 9 December 2004

Phospholipase Cε is a novel class of phosphoinositide-specific phospholipase C, identified as a downstream effector of Ras and Rap small GTPases. We report here the first genetic analysis of its physiological function with mice whose phospholipase Cε is catalytically inactivated by gene targeting. The hearts of mice homozygous for the targeted allele develop congenital malformations of both the aortic and pulmonary valves, which cause a moderate to severe degree of regurgitation with mild stenosis and result in ventricular dilation. The malformation involves marked thickening of the valve leaflets, which seems to be caused by a defect in valve remodeling at the late stages of semilunar valvulogenesis. This phenotype has a remarkable resemblance to that of mice carrying an attenuated epidermal growth factor receptor or deficient in heparin-binding epidermal growth factor-like growth factor. Smad1/5/8, which is implicated in proliferation of the valve cells downstream of bone morphogenetic protein, shows aberrant activation at the margin of the developing semilunar valve tissues in embryos deficient in phospholipase Cε. These results suggest a crucial role of phospholipase Cε downstream of the epidermal growth factor receptor in controlling semilunar valvulogenesis through inhibition of bone morphogenetic protein signaling.

The hydrolysis of phosphatidylinositol 4,5-bisphosphate (PIP_2) by phosphoinositide-specific phospholipase C (PLC) is a key event triggering intracellular signal transduction from various receptor molecules at the plasma membrane by yielding two intracellular second messengers, diacylglycerol and inositol 1,4,5-trisphosphate, which induce activation of protein kinase C and mobilization of Ca^{2+} from intracellular stores, respectively (9). Concurrently, reduction in PIP_2 concentration appears to be an important signal because activities of various actin-binding proteins and pleckstrin homology domain-containing proteins are modulated through interaction with PIP_2 (25). More than 12 mammalian PLC isoforms have been identified and organized into five classes (β, γ, δ, ε, and ζ), which are regulated through distinct mechanisms (9). PLCε is characterized by possession of two Ras-associating domains and a CDC25 homology domain. The Ras-associating domains are responsible for activation of PLCε through direct association with the GTP-bound active forms of the small GTPases Ras (15, 23), Rap1 (23, 24), and Rap2 (20). Stimulation of cells by growth factors, such as platelet-derived growth factor, induces persistent activation of PLCε through activation of Ras and Rap1 (24). The rapid and initial phase of this activation is mediated by Ras at the plasma membrane, whereas Rap1 is responsible for the prolonged activation mainly at the Golgi complex (24). The CDC25 homology domain acts as a guanine nucleotide exchange factor for Rap1 and is crucial for the prolonged activation of PLCε by Rap1 (14, 24). The involvement of other factors, such as the α subunits of the G_{12} and G_{13} families or the $\beta_1\gamma_2$ subunits of heterotrimeric G proteins (18, 29) and Rho small GTPase (30), in regulation of PLCε was also reported, but their underlying mechanisms still remain unclear. Although the molecular mechanism of PLCε regulation has been intensively studied, little is known about its physiological function. Because multiple isoforms of PLCs are usually expressed in a single cell, functional analysis of an individual isoform needs a targeted disruption of the corresponding gene. These analyses with β and δ isoforms have been successful in elucidating their distinct and cell-type-specific roles (9). In this paper, we show that PLCε is required for proper formation of the semilunar valves by generation and phenotypic characterization of mice whose PLCε is genetically inactivated.

* Corresponding author. Mailing address: Division of Molecular Biology, Department of Molecular and Cellular Biology, Kobe University Graduate School of Medicine, 7-5-1 Kusunoki-cho, Chuo-ku, Kobe 650-0017, Japan. Phone: 81-78-382-5380. Fax: 81-78-382-5399. E-mail: kataoka@kobe-u.ac.jp.

‡ M.T. and H.E. contributed equally to this work.

† Supplemental material for this article may be found at http://mcb.asm.org/.

MATERIALS AND METHODS

Construction of a targeting vector. The *PLC*ε genomic gene was cloned from a 129/Sv mouse genomic library, and a 10.2-kb fragment harboring the exons encoding the catalytic X domain of PLCε was used for construction of the targeting vector. An internal 3-kb region containing the 3′ part of one of four

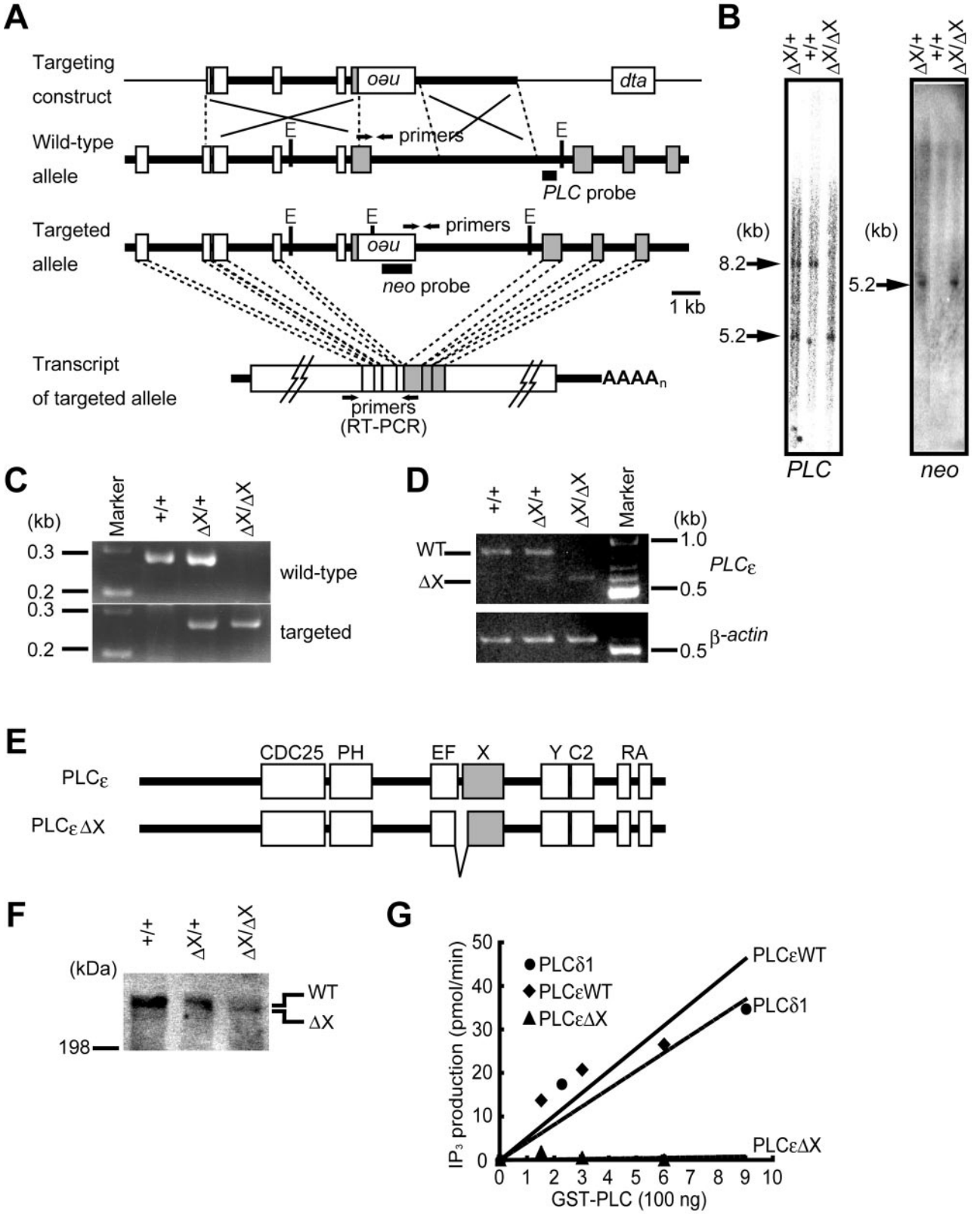

FIG. 1. Targeted disruption of the mouse *PLC*ε gene. (A) Schematic representation of the structure of the targeting construct, the wild-type allele, and the targeted allele. The targeting construct carries the inverted *PGK-neo* cassette (*neo*) and the diphtheria toxin A chain cassette (*dta*). Boxes represent the exons. The exons encoding the X domain are shaded. Positions of the primers for PCR or RT-PCR, EcoRV cleavage sites (E), and the probes for Southern blot analysis, *PLC* and *neo* probes, are indicated. (B) Southern blot analysis of genomic DNA. Genomic DNAs isolated from the *PLC*ε$^{+/+}$ (+/+), *PLC*ε$^{\Delta X/+}$ (ΔX/+), and *PLC*ε$^{\Delta X/\Delta X}$ (ΔX/ΔX) mouse tails were digested with EcoRV, followed by Southern blot

exons encoding the X domain was replaced with an inverted *PGK-neo* cassette for positive selection, in which expression of the neomycin-resistance gene is driven by the phosphoglycerate kinase promoter (Fig. 1A). The targeting vector also possessed the diphtheria toxin A chain cassette for negative selection.

Gene targeting and generation of mutant mice. To generate the targeted *PLC*ε allele, designated *PLC*$\varepsilon^{\Delta X}$, mouse embryonic stem (ES) cells derived from 129/Sv strain were transfected with the linearized targeting vector by electroporation and subsequently subjected to selection with G418. The G418-resistant clones were isolated and screened by Southern blot analysis of their EcoRV-cleaved genomic DNAs with the probes depicted in Fig. 1A. Out of more than 1,000 clones analyzed, only 1 ES clone carried the properly generated *PLC*$\varepsilon^{\Delta X}$ allele and was injected into mouse C57BL/6 blastocysts to generate a chimeric male, which was subsequently bred with C57BL/6 females to generate heterozygous mice. Homozygous mutant mice were generated by cross-breeding of heterozygous mice. Mice were maintained on a hybrid of 129/Sv and C57BL/6, and their genotypes were determined within 3 weeks after birth by PCR with allele-specific primers (5′-CATGTGTCATCAAGGCCTAC-3′ and 5′-CTATAGAGC TCCACAGAGGACTC-3′ for the wild-type allele; 5′-GAATGTGTGCGAGG CCGAAGG-3′ and 5′-GCTATGTAAGCCTGGAATTGCATC-3′ for the targeted allele). To obtain *PLC*$\varepsilon^{\Delta X/\Delta X}$ embryos, female *PLC*$\varepsilon^{\Delta X/+}$ mice were placed together with a male *PLC*$\varepsilon^{\Delta X/+}$ mouse overnight. The next noon was defined as embryonic day 0.5 (E0.5). The genotypes of embryos were determined similarly by PCR with genomic DNA isolated from their extraembryonic membranes. All animals were maintained at the animal facilities of Kobe University Graduate School of Medicine according to institutional guidelines.

Reverse transcription (RT)-PCR analysis. Total cellular RNA was prepared from mouse hearts with TRIzol reagent (Invitrogen), and the first-strand oligo(dT)-primed cDNA was synthesized as previously described (31). Primers used for amplification of *PLC*ε were 5′-TCAGTGCCTGGAGCAGCAG-3′ and 5′-C TTGAAGGGGATCTTGGTTG-3′, and those for β-*actin* were described previously (31).

Western blot analyses. Protein was extracted from the cerebellum of adult mice with lysis buffer (50 mM Tris-HCl [pH 7.4], 200 mM NaCl, 1% [vol/vol] NP-40, 1.5 μg of leupeptin/ml, 1.5 μg of aprotinin/ml). Protein concentrations were determined by the Bradford method (Bio-Rad). Western blotting with the anti-mouse PLCε antibody was performed as described previously (31).

In vitro PLC assay. Fragments of mouse PLCε consisting of its X, Y, and C2 domains (amino acids 1280 to 1943 for the wild type and amino acids 1280 to 1332 and 1409 to 1943 for the deletion mutant) were expressed as fusions with *Schistosoma japonicum* glutathione *S*-transferase (GST) in *Escherichia coli* BL21(DE3) by using pGEX6P-1 (Amersham Biosciences) and purified with glutathione-Sepharose resin (Amersham Biosciences). Full-length rat PLCδ1 (PLCδ1) was also produced and purified as a GST fusion protein (22*)*. Their PIP_2-hydrolyzing activities were determined as described previously (22).

Histochemistry. Newborn mice and embryos were fixed in 10% formalin in phosphate-buffered saline at 4°C overnight. For histological analyses of tissues of adult mice, paraffin-embedded sections were prepared and stained with hematoxylin and eosin (H&E). For examination of fibrosis of the heart, azan staining was performed on paraffin-embedded 5-μm-thick transverse serial sections. To analyze the hearts of embryos, standard H&E staining was performed on 6-μm-thick serial transverse cryosections. The thickness of the semilunar valves was measured on two or three leaflets per each valve of individual embryos and averaged. The size of semilunar valve cells was calculated by dividing the area of the valve leaflet by the number of nuclei stained with H&E, both of which were determined with a digital microscope (VH-8000; Keyence, Osaka, Japan). For immunohistochemical analyses with confocal laser microscopes (LSM510 META; Zeiss, Jena, Germany), cryosections were pretreated with 10 μg of proteinase K /ml of phosphate-buffered saline containing 0.1% Triton X-100 for 15 min, followed by blocking with 1% bovine serum albumin for 1 h. The sections were then treated with a primary antibody specific to PLCε (31), phospho-Smad1(Ser463/465)/Smad5(Ser463/465)/Smad8(Ser426/428) (catalogue no. 9551; Cell Signaling Technology, Inc.), cleaved caspase-3 (catalogue no. 9661; Cell Signaling Technology, Inc.), phospho-p44/42 mitogen-activated protein kinase (Thr202/Tyr204) (catalogue no. 9106; Cell Signaling Technology, Inc.), phospho-epidermal growth factor (phospho-EGF) receptor, ErbB1 (Tyr1173) (catalogue no. sc-12351; Santa Cruz Biotechnology, Inc.), proliferating cell nuclear antigen (catalogue no. M0879; Dako Cytomation), or Ki-67 (catalogue no. RB-081A0; Neo Markers) at 4°C overnight and subsequently treated with Alexa Fluor 488-labeled anti-rabbit immunoglobulin G and/or Alexa Fluor 546-labeled anti-mouse immunoglobulin G (Molecular Probes, Inc.) or with fluorescein-labeled anti-rabbit immunoglobulin G (Chemicon) and Alexa Fluor 546-labeled anti-goat immunoglobulin G for 1 h. A TdT-mediated dUTP nick end labeling assay was performed on proteinase K-treated cryosections with an in situ cell death detection kit (Roche Diagnostics Corp.). Nuclear staining with 4′6-diamino-5-phenylindole (DAPI) was carried out as previously described (31).

Echocardiographic analysis. Mice were anesthetized with Avertin administered intraperitoneally at 250 μg/g of body weight. Transthoracic echocardiography was performed with a Toshiba Aplio instrument along with a 14-MHz linear transducer (PLT-1202S; Toshiba). Left ventricular internal dimension at end-diastole and end-systole (LVIDd and LVIDs, respectively), interventricular septal thickness at end-diastole, and left ventricular posterior wall thickness at end-diastole were measured on M-mode images. The percent fractional shortening (% FS) and heart rate-corrected mean velocity of circumferential fiber shortening (mVcfc) were calculated as $\%\ FS = 100 \times (LVIDd - LVIDs)/LVIDd$ and $mVcfc = \%\ FS \times (\text{cycle length})^{1/2}/\text{duration of aortic valve opening}$.

Velocities of aortic outflow and diastolic transmitral left ventricular inflow were measured from angulated parasternal long-axis views obtained by a 6.6-MHz pulsed-wave Doppler transducer with a sample volume length of 1.0 mm. To measure the velocity of aortic or pulmonary flow, the sample volume was fixed about 1 mm above the semilunar valves as a guide of color flow-mapping Doppler. Attempts were made to align the ultrasound beam as parallel as possible to flow and to record the highest velocities.

In vivo hemodynamic study. Mice were anesthetized with Avertin (250 μg/g), and their trachea and right carotid artery were exposed. Mice were then intubated with a blunt 21-gauge-needle tube and connected to a volume-cycled rodent ventilator (SN-480-7; SHINANO) with a tidal volume of 0.2 ml and a respiratory rate of 100 beats/min. A 1.4-F microtip catheter (SPR671; Millar Instruments) was inserted retrograde into the left ventricle through the right carotid artery. Data were collected with an analog-to-digital converter (Power Laboratory; ADInstruments) and recorded (Chart, version 4; ADInstruments) in real time. The maximal pressure gradient between the maximal systolic pressure of the left ventricle and that of the aorta was measured by pulling the catheter back from the left ventricle to the aorta and averaged from three to five consecutive beats of left ventricle and aortic pressures.

Statistical analysis. Values are expressed as means ± standard error. The unpaired Student *t* test with Welch correction was performed to determine *P* values with GraphPad InStat software (GraphPad Software, Inc.). If *P* values were <0.05, differences were considered to be statistically significant.

RESULTS

Generation of *PLC*$\varepsilon^{\Delta X/\Delta X}$ mice. We generated a targeted *PLC*ε allele, designated *PLC*$\varepsilon^{\Delta X}$, by replacing the 3′ part of one of four exons encoding the X domain with the *PGK-neo* cassette in mouse 129/Sv-derived ES cells. Out of more than 1,000 G418-resistant ES clones, only one clone carried the properly targeted *PLC*ε allele and was used for the generation of mutant mice (data not shown). Hybridization of the EcoRV-

analysis with a *PLC* probe (left) or *neo* probe (right). The positions and sizes of the hybridization signals are indicated. (C) Genotyping by PCR. Genomic DNAs were analyzed by PCR using the allele-specific primers. (D) RT-PCR analysis of the *PLC*ε mRNA expressed in the heart. Two PCR products, 829 and 676 bp, were amplified from the transcripts of the wild-type (WT) and *PLC*$\varepsilon^{\Delta X}$ (ΔX) alleles, respectively. β-*actin* mRNA was used as an internal control. (E) Schematic representation of the structures of wild-type PLCε and its mutant protein expressed from the *PLC*$\varepsilon^{\Delta X}$ allele (PLCεΔX). (F) Western blot analysis of PLCεΔX protein expression. Expression of the wild type and ΔX mutant of PLCε was analyzed by Western blotting of proteins (100 μg each) extracted from the cerebella of adult mice with the anti-mouse PLCε antibody. The positions of the wild type (WT) and ΔX mutant (ΔX) are indicated. (G) Enzymatic activity of *PLC*εΔX mutant. GST fusions of the wild type (PLCεWT), mutant PLCε (PLCεΔX), and PLCδ1 were incubated with ^{3}H-labeled PIP_2, and production of ^{3}H-labeled inositol-1,4,5-trisphosphate was measured. The specific activities of PLCεWT, PLCδ1, and PLCεΔX were 51, 41, and 0.76 nmol/mg/min, respectively. Representative results of three independent experiments are shown.

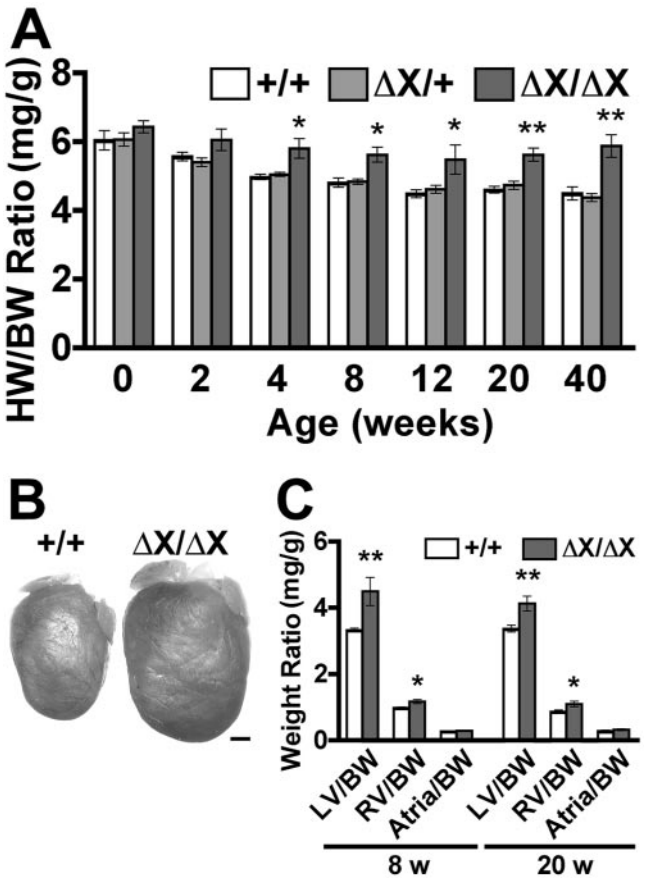

FIG. 2. Heart enlargement in $PLC\varepsilon^{\Delta X/\Delta X}$ mice. (A) Heart-to-body weight (HW/BW) ratios. At least nine mice of each genotype were examined at the times indicated. (B) Representative images of the hearts of 20-week-old female littermates, $PLC\varepsilon^{+/+}$ (+/+) and $PLC\varepsilon^{\Delta X/\Delta X}$ (ΔX/ΔX). Scale bar, 1 mm. (C) Weight ratios between the different heart compartment and the body. The heart was divided into the left ventricle (LV), right ventricle (RV), and atria, which were separately weighed. Nine mice of each genotype were examined at the indicated ages. *, $P < 0.05$; **, $P < 0.01$.

digested genomic DNAs from the mouse tails with a *PLC*ε allele-specific probe (*PLC* probe) identified a 5.2-kb band of the $PLC\varepsilon^{\Delta X}$ allele in homozygous ($PLC\varepsilon^{\Delta X/\Delta X}$) and heterozygous ($PLC\varepsilon^{\Delta X/+}$) mice and a 8.2-kb band of the wild-type allele in wild-type ($PLC\varepsilon^{+/+}$) and $PLC\varepsilon^{\Delta X/+}$ mice, both of which coincided with those predicted from the gene structure (Fig. 1A and B). Hybridization of the same DNAs with a *PGK-neo* cassette-specific probe (*neo* probe) identified only a 5.2-kb band in $PLC\varepsilon^{\Delta X/\Delta X}$ and $PLC\varepsilon^{\Delta X/+}$ mice, indicating the absence of an extracopy integration of the *PGK-neo* cassette (Fig. 1A and B). The $PLC\varepsilon^{\Delta X}$ allele was also verified by PCR. Targeted allele-specific primers amplified a 270-bp product of the predicted size from $PLC\varepsilon^{\Delta X/\Delta X}$ and $PLC\varepsilon^{\Delta X/+}$ mouse genomic DNA (Fig. 1A and C). RT-PCR analysis of the heart mRNA revealed the existence of a shortened *PLC*ε mRNA in $PLC\varepsilon^{\Delta X/\Delta X}$ and $PLC\varepsilon^{\Delta X/+}$ mice (Fig. 1D). Sequence determination of the 676-bp PCR product amplified from the transcript of the $PLC\varepsilon^{\Delta X}$ allele revealed deletion of another upstream exon, which was presumably caused by exon skipping upon RNA splicing (Fig. 1D). This resulted in production of a

TABLE 1. Summary of M-mode echocardiographic analysis[a]

Test or characteristic	Age and *PLC*ε genotype			
	8 wk		20 wk	
	+/+	ΔX/ΔX	+/+	ΔX/ΔX
Heart rate (min^{-1})	419 ± 16	408 ± 13	400 ± 18	386 ± 14
LVIDd (mm)	3.6 ± 0.1	4.2 ± 0.2*	4.0 ± 0.2	4.4 ± 0.1*
LVIDs (mm)	2.2 ± 0.1	2.9 ± 0.2**	2.7 ± 0.1	3.0 ± 0.1
% FS	37.7 ± 1.5	32.1 ± 1.4**	32.8 ± 1.6	31.9 ± 0.9
IVSd (mm)	0.7 ± 0.0	0.7 ± 0.0	0.7 ± 0.0	0.8 ± 0.1
LVPWd (mm)	0.7 ± 0.0	0.7 ± 0.0	0.7 ± 0.0	0.7 ± 0.0
mVcfc (mm/s)	6.3 ± 0.3	4.8 ± 0.4**	5.0 ± 0.4	4.8 ± 0.2
Total no. of mice analyzed	15	15	9	9

[a] Abbreviations: LVIDd, left ventricular internal dimension at end-diastole; LVIDs, left ventricular dimension at end-systole; FS, fractional shortening; IVSd, interventricular septal thickness at end-diastole; LVPWd, left ventricular posterior wall thickness at end-diastole; mVcfc, heart rate-corrected mean velocity of circumferential fiber shortening. *, $P < 0.05$; **, $P < 0.01$ between $PLC\varepsilon^{+/+}$ and $PLC\varepsilon^{\Delta X/\Delta X}$ mice.

PLCε mutant carrying an in-frame deletion of amino acids 1333 to 1408, as illustrated in Fig. 1E. Western blot analysis of cell extracts of the $PLC\varepsilon^{\Delta X/\Delta X}$ and $PLC\varepsilon^{\Delta X/+}$ mouse cerebella with the anti-PLCε antibody recognizing its C terminus revealed residual expression of the mutant PLCε (PLCεΔX) in the mutant mice (Fig. 1F). The deletion encompasses the N-terminal part of the X domain, which contains essential residues for the enzymatic activity of PLC (5, 7, 8). In fact, the specific activities of the wild-type and mutant proteins were determined to be 51 and 0.76 nmol/min/mg of protein, respectively, by an in vitro assay employing their recombinant GST fusion polypeptides consisting of the X, Y, and C2 domains, demonstrating that this deletion completely abrogated PIP_2-hydrolyzing activity (Fig. 1G).

Ventricular dilation in $PLC\varepsilon^{\Delta X/\Delta X}$ mice. Expression of *PLC*ε mRNA was detected at various levels in almost all the tissues in mammals (15, 18, 31). We had shown by in situ hybridization analyses that PLCε is highly expressed in developing neural tissues and skeletal muscle tissues in mouse embryos (31) and by immunohistochemical analyses that *PLC*ε is highly expressed in neurons in the brain and modestly in the skin, skeletal muscles, and heart of adult mice (1, 31; data not shown). Therefore, we expected that inactivation of PLCε might result in defects of these organs. However, $PLC\varepsilon^{\Delta X/\Delta X}$ pups were born at normal Mendelian ratios ($PLC\varepsilon^{+/+}$:$PLC\varepsilon^{\Delta X/+}$:$PLC\varepsilon^{\Delta X/\Delta X}$ = 26.4%:49.4%:24.2%; 632 pups) without any intrauterine loss or early death; the pups were fertile and indistinguishable from their $PLC\varepsilon^{+/+}$ or $PLC\varepsilon^{\Delta X/+}$ littermates in appearance and growth (data not shown). They grew normally for at least 2 years. However, anatomical examination revealed that their hearts were enlarged compared with those of $PLC\varepsilon^{+/+}$ and $PLC\varepsilon^{\Delta X/+}$ mice (Fig. 2A and B), while other organs, including neuronal tissues that express PLCε at a high level (31), appeared anatomically and histologically normal (data not shown). The heart-to-body weight ratio of $PLC\varepsilon^{\Delta X/\Delta X}$ mice was greater than those of $PLC\varepsilon^{+/+}$ and $PLC\varepsilon^{\Delta X/+}$ mice, even on postnatal day 1 (P1) (Fig. 2A), and the difference showed a considerable increase to approximately 1.4-fold by 40 weeks after birth (Fig. 2A). No difference was observed between $PLC\varepsilon^{+/+}$ and $PLC\varepsilon^{\Delta X/+}$ mice (Fig. 2A). The $PLC\varepsilon^{\Delta X/\Delta X}$ hearts showed weight increases in both the left

TABLE 2. Summary of hemodynamic analysis[a]

Test or characteristic	Result for indicated *PLC*ε genotype at age:			
	8 wk		20 wk	
	+/+	ΔX/ΔX	+/+	ΔX/ΔX
LVP (mm Hg)	83 ± 6	95 ± 4	88 ± 3	108 ± 7*
EDP (mm Hg)	3.1 ± 0.9	2.4 ± 0.7	2.0 ± 0.7	3.9 ± 1.0
dP/dt_{max} (× 10^3 mm Hg/s)	8.7 ± 1.0	7.2 ± 0.9	6.8 ± 0.8	7.1 ± 0.5
dP/dt_{min} (× 10^3 mm Hg/s)	−5.7 ± 0.7	−4.8 ± 0.5	−6.2 ± 0.7	−6.3 ± 0.6
AP_{max} (mm Hg)	80 ± 6	72 ± 5	87 ± 3	82 ± 5
AP_{min} (mm Hg)	38 ± 5	30 ± 5	47 ± 5	45 ± 6
PG (mm Hg)	3.4 ± 0.6	22.8 ± 4.5**	1.2 ± 1.0	26.2 ± 4.0**
Total no. of mice analyzed	9	10	8	6

[a] Abbreviations: LVP, maximal left ventricular pressure; EDP, left ventricular end-diastolic pressure; dP/dt_{max}, maximal first derivative of the change in left ventricular pressure/time (pressure development); dP/dt_{min}, minimum first derivative of the change in left ventricular pressure/time (pressure relaxation); AP_{max}, maximal aortic pressure; AP_{min}, minimal aortic pressure; PG, pressure gradient across the aortic valve. *, $P < 0.05$; **, $P < 0.01$ between $PLC\varepsilon^{+/+}$ and $PLC\varepsilon^{\Delta X/\Delta X}$ mice.

and right ventricles, but not in the atria (Fig. 2C). Similar results were obtained after five generations of backcrossing of this mutant mouse line with a wild-type C57BL/6 strain, indicating that the cardiac phenotype observed here is independent of the genetic background and is not due to artifacts that might have arisen from gene targeting (see Fig. S1 in the supplemental data). Analysis by M-mode echocardiography revealed that LVIDs at both end-diastole and end-systole of $PLC\varepsilon^{\Delta X/\Delta X}$ mice were greater than those of $PLC\varepsilon^{+/+}$ mice at 8 or 20 weeks of age (Table 1). In contrast, interventricular septal thickness and left ventricular posterior wall thickness at end-diastole showed no significant difference (Table 1). These results indicated that the observed heart enlargement was mainly due to ventricular dilation rather than hypertrophy. Consistent with this, histological analysis of azan-stained sections revealed no structural abnormality or fibrosis in the left ventricles of $PLC\varepsilon^{\Delta X/\Delta X}$ mice (data not shown).

Ventricular dilation of $PLC\varepsilon^{\Delta X/\Delta X}$ mice is caused by regurgitation of the semilunar valves. Although some parameters of contractility, such as FS and mVcfc, appeared to be reduced in $PLC\varepsilon^{\Delta X/\Delta X}$ mice at 8 weeks of age (Table 1), no obvious abnormality was found in pressure development, left ventricular end-diastolic pressure, and pressure relaxation at both 8 and 20 weeks of age (Table 2), indicating that the systolic and diastolic functions of the $PLC\varepsilon^{\Delta X/\Delta X}$ hearts were almost normal. However, Doppler echocardiographic analysis revealed that the $PLC\varepsilon^{\Delta X/\Delta X}$ hearts clearly suffered from moderate to severe degrees of regurgitation of both the aortic valve (Fig. 3A; see Fig. S2 in the supplementary data) and pulmonary valve (see Fig. S2 in the supplementary data) at the diastolic phase. The pulsed-wave Doppler also revealed that flow velocity across the $PLC\varepsilon^{\Delta X/\Delta X}$ aortic valve was abnormally fast (Fig. 3B), indicating the presence of aortic stenosis. Transvalvular pressure gradients across the aortic, pulmonary, and mitral valves at the systolic phase were estimated from the flow velocities. Transvalvular pressure gradient across the aortic valve was around 20 mm Hg in $PLC\varepsilon^{\Delta X/\Delta X}$ mice (Table 3), indicating a mild degree of aortic stenosis. This was also evidenced from the results of pressure measurement by a pullback of a catheter from the left ventricle to the aorta (Fig. 3C; Table 2). Transvalvular pressure gradient across the pulmonary valve was also significantly high at 20 weeks (Table 3). These results indicated that $PLC\varepsilon^{\Delta X/\Delta X}$ mice suffered not only from regurgitation but also from stenosis at the semilunar valves. On the other hand, the mitral valves were almost unaffected in $PLC\varepsilon^{\Delta X/\Delta X}$ mice (Table 3). Taken together, the cardiac dilation of $PLC\varepsilon^{\Delta X/\Delta X}$ mice was likely to be caused by chronic volume overload due mainly to semilunar valve regurgitation.

Thickening of the semilunar valve leaflets in $PLC\varepsilon^{\Delta X/\Delta X}$ mice. Echocardiographic analysis revealed that the diameters of the semilunar valve orifices at the systolic phase were normal in $PLC\varepsilon^{\Delta X/\Delta X}$ mice (Table 3). However, an anatomical examination of $PLC\varepsilon^{\Delta X/\Delta X}$ hearts of 20 weeks of age revealed that the sizes of the leaflets became uneven and the individual leaflet of the aortic valve exhibited marked thickening, although the aortic valve still maintained a three-leaved structure (Fig. 4A). Some of the $PLC\varepsilon^{\Delta X/\Delta X}$ aortic valves at 40 weeks of age exhibited a bicuspid-like appearance due to commissural fusion (Fig. 4B). This may suggest that the valve thickening aggravates an age-dependent deformation process. As observed with the heart weight increase, the valve malformation in $PLC\varepsilon^{\Delta X/\Delta X}$ mice was unaffected by five generations of backcross with C57BL/6 mice (see Fig. S3 in the supplemental data). We next analyzed which stage of the valve formation was disturbed in $PLC\varepsilon^{\Delta X/\Delta X}$ mice during embryogenesis because a sign of heart enlargement was observed in newborn mice (Fig. 2B). On E15.5, the shape of the semilunar valves, as well as the septation of the aortic and pulmonary trunks and interventricles, of $PLC\varepsilon^{\Delta X/\Delta X}$ mice were indistinguishable from those of $PLC\varepsilon^{+/+}$ mice (Fig. 4C and data not shown), indicating that the early stages of valvular and septal formation, including endocardial cushion formation, proceeded normally without PLCε. However, the subsequent valvular remodeling step was obviously disturbed: while the immature aortic and pulmonary valves of $PLC\varepsilon^{+/+}$ mice underwent remodeling to form slender leaflets on E16.5, those of $PLC\varepsilon^{\Delta X/\Delta X}$ mice still maintained thickened leaflets at E16.5 and later (Fig. 4 and data not shown). Moreover, both the aortic and pulmonary valves of $PLC\varepsilon^{\Delta X/\Delta X}$ mice underwent a massive increase in thickness on E16.5 (Fig. 4D). The thickening of the aortic and pulmonary valves of $PLC\varepsilon^{\Delta X/\Delta X}$ mice appeared to be due to an increase in the number of cells, because PLCε deficiency did not alter cell size (Fig. 4E). In the tricuspid and mitral valves, no apparent difference existed between $PLC\varepsilon^{+/+}$ and

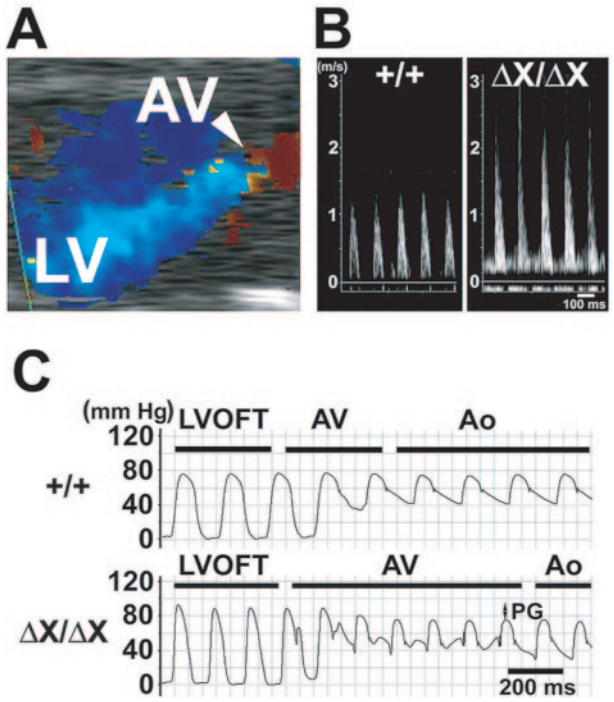

FIG. 3. Functional analyses of *PLC*ε$^{\Delta X/\Delta X}$ mouse hearts. (A) Color flow-mapping Doppler echocardiograph of the *PLC*ε$^{\Delta X/\Delta X}$ mouse heart at the diastolic phase showing the aortic valve (AV) and the left ventricle (LV). The blue color represents that backward flow through the aortic valve reaches the apex of the left ventricle, suggesting massive aortic regurgitation. The movie clip of the color flow-mapping Doppler echocardiograph of this mouse is also available as in the supplemental data as Fig. S2. (B) Representative pulsed-wave Doppler echocardiographic images of the flow velocity across the aortic valve of *PLC*ε$^{+/+}$ (+/+) and *PLC*ε$^{\Delta X/\Delta X}$ (ΔX/ΔX) mice. (C) Representatives of the measurement of withdrawal pressure across the aortic valve. Pressure measurements of 20-week-old female *PLC*ε$^{+/+}$ (+/+) and *PLC*ε$^{\Delta X/\Delta X}$ (ΔX/ΔX) mice were performed by a pullback of a catheter from the left ventricular outflow tract (LVOFT) to the aorta through the aortic valve. PG, pressure gradient; AV, aortic valve; Ao, aorta.

TABLE 3. Summary of Doppler echocardiographic analysis[a]

Test or characteristic	Result for indicated *PLC*ε genotype at age:			
	8 wk		20 wk	
	+/+	ΔX/ΔX	+/+	ΔX/ΔX
AVD (mm)	1.1 ± 0.0	1.3 ± 0.1	1.4 ± 0.1	1.5 ± 0.1
AVV (m/s)	1.2 ± 0.1	2.3 ± 0.4*	1.3 ± 0.0	2.2 ± 0.2**
AVPG (mm Hg)	5.6 ± 0.8	23.9 ± 8.6*	6.8 ± 0.4	20.1 ± 4.0**
Mice with AR	0	5	0	4
PVD (mm)	1.3 ± 0.0	1.3 ± 0.0	1.5 ± 0.1	1.6 ± 0.1
PVV (m/s)	0.6 ± 0.1	0.7 ± 0.1	0.8 ± 0.0	1.1 ± 0.1*
PVPG (mm Hg)	1.8 ± 0.3	2.2 ± 0.3	2.4 ± 0.2	4.6 ± 1.0*
Mice with PR	0	5	0	4
MVD (mm)	1.7 ± 0.2	1.8 ± 0.1	1.7 ± 0.1	1.8 ± 0.1
MVV (m/s)	0.7 ± 0.1	0.6 ± 0.1	0.5 ± 0.1	0.5 ± 0.1
MVPG (mm Hg)	2.0 ± 0.3	1.6 ± 0.5	1.1 ± 0.2	1.2 ± 0.5
Mice with MR	0	1	0	0
Total no. of mice analyzed	5	5	6	4

[a] Abbreviations: AVD, aortic valve orifice diameter; AVV, maximal flow velocity across the aortic valve; AVPG, estimated pressure gradient across the aortic valve; AR, aortic valve regurgitation; PVD, pulmonary valve orifice diameter; PVV, maximal flow velocity across the pulmonary valve; PVPG, estimated pressure gradient across the pulmonary valve; PR, pulmonary valve regurgitation; MVD, mitral valve orifice diameter; MVV, maximal flow velocity across the mitral valve; MVPG, estimated pressure gradient across the mitral valve; MR, mitral valve regurgitation. *, $P < 0.05$; **, $P < 0.01$ between *PLC*ε$^{+/+}$ and *PLC*ε$^{\Delta X/\Delta X}$ mice.

*PLC*ε$^{\Delta X/\Delta X}$ mice throughout valvulogenesis (data not shown). These results suggest that PLCε may play a role in regulation of proliferation or apoptosis of the semilunar valve cells at the late stages of valvulogenesis.

The semilunar valve phenotypes of *PLC*ε$^{\Delta X/\Delta X}$ mice are almost identical to those of mice deficient in HB-EGF or its receptor. PLCε is expressed all over the valve areas, both semilunar and atrioventricular, with high levels of expression at their margins (Fig. 5A and data not shown). In addition, PLCε is also expressed in myocardium as reported previously (31). The PLCεΔX mutant protein is expressed in the *PLC*ε$^{\Delta X/\Delta X}$ heart in a similar fashion (Fig. 5A). The semilunar valve malformation of *PLC*ε$^{\Delta X/\Delta X}$ mice showed a remarkable resemblance to the phenotypes of mice deficient in heparin-binding (HB) EGF-like growth factor (HB-EGF) or its receptor ErbB1, the EGF receptor (4, 11, 12). The mice deficient in HB-EGF exhibit severe semilunar valve dysfunctions (11, 12) due to marked thickening of the valve leaflets, leading to early death of 60% of the newborn pups before weaning (12). Considering that PLCε is activated by ErbB1-mediated signaling through activation of Ras or Rap (14, 23, 24), we anticipated a direct link between PLCε and HB-EGF signaling upon semilunar valvulogenesis. Thus, cells in the valve leaflets were examined for proliferation by the expression of proliferating cell nuclear antigen or Ki-67 antigen and for apoptosis by TdT-mediated dUTP nick end labeling assay or by immunodetection of active caspase-3. However, we could not observe any significant difference in the number of cells undergoing proliferation or apoptosis between *PLC*ε$^{+/+}$ and *PLC*ε$^{\Delta X/\Delta X}$ mice (data not shown). Because HB-EGF-deficient mice were reported to exhibit only a modest increase in proliferating cells compared to wild-type mice (12), it is not unexpected that we failed to observe a significant increase in *PLC*ε$^{\Delta X/\Delta X}$ mice, exhibiting a milder valve thickening.

Aberrant activation of Smad1/5/8 in the developing semilunar valve leaflets of *PLC*ε$^{\Delta X/\Delta X}$ mice. Proliferation of the heart valve cells was reported to be positively controlled by bone morphogenetic protein signaling-mediated activation and negatively controlled by ErbB1-mediated suppression, of receptor-regulated Smad, Smad1/5/8 (21). Thus, we analyzed the level of the Smad1/5/8 activation by immunohistochemistry with an antibody specific to Smad1/5/8 phosphorylated at the C terminus. In the *PLC*ε$^{+/+}$ pulmonary valves, cells positive for phospho-Smad1/5/8 preferentially resided at the margins of the developing valves on E13.5 through E14.5, and the frequency of the phospho-Smad1/5/8-positive cells did not increase significantly during this period (Fig. 5B and C). On E15.5, the number of phospho-Smad1/5/8-positive cells increased in the marginal region of the pulmonary valves (Fig. 5B and C). In the *PLC*ε$^{\Delta X/\Delta X}$ pulmonary valves on E13.5, the distribution

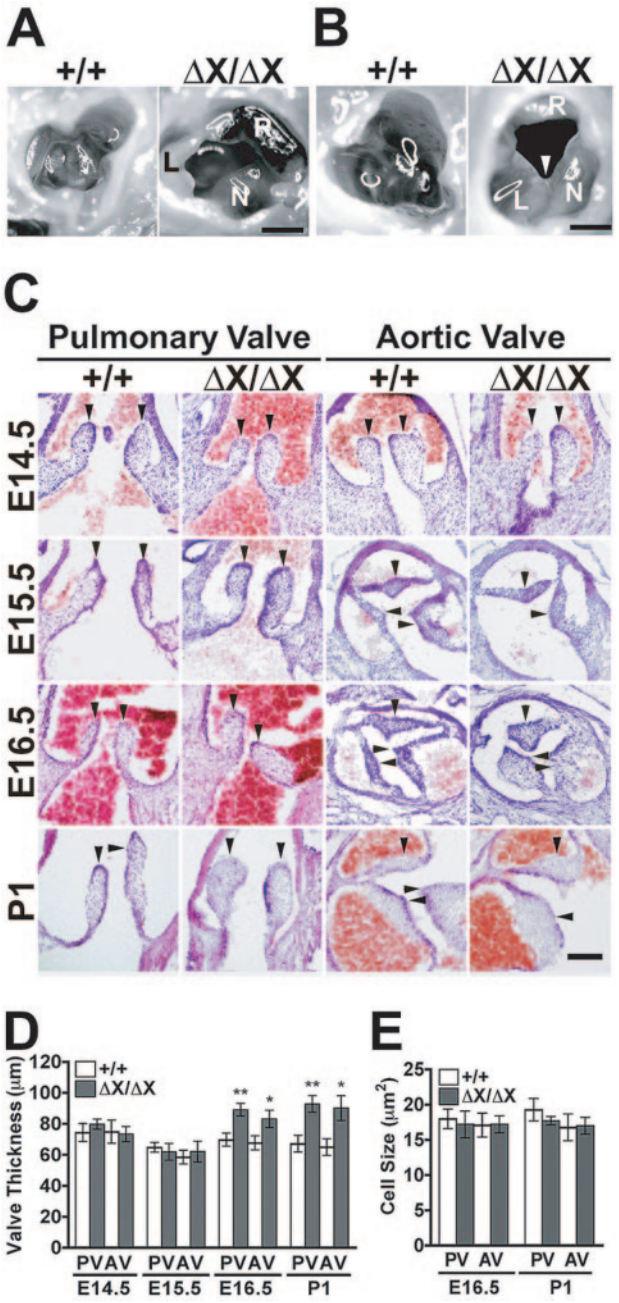

FIG. 4. Semilunar valve defects in *PLC*ε$^{\Delta X/\Delta X}$ mice. (A) The aortic valves of 20-week-old female littermates of *PLC*ε$^{+/+}$ (+/+) and *PLC*ε$^{\Delta X/\Delta X}$ (ΔX/ΔX) mice. The *PLC*ε$^{\Delta X/\Delta X}$ aortic valve exhibits thickening and uneven formation of the valve leaflets. Abbreviations: L, left coronary cusp; N, noncoronary cusp; R, right coronary cusp. Scale bar, 200 μm. (B) The aortic valves of 40-week-old male littermates of *PLC*ε$^{+/+}$ (+/+) and *PLC*ε$^{\Delta X/\Delta X}$ (ΔX/ΔX) mice. The white arrowhead indicates the commissural fusion of left coronary cusp and noncoronary cusp. Abbreviations: L, left coronary cusp; N, noncoronary cusp; R, right coronary cusp. Scale bar, 200 μm. (C) H&E staining of transverse sections of the hearts of littermate embryos (E14.5 to E16.5) and newborn mice (P1). Arrowheads indicate the semilunar valve leaflets. Scale bar, 100 μm. (D) Measurement of the thickness of the pulmonary and aortic valves (PV and AV, respectively). At least five embryos or newborn mice (P1) of each genotype were examined at each time point. (E) Sizes of semilunar valve cells. At least four embryos of each genotype of E16.5 and P1 were analyzed. *, $P < 0.05$; **, $P < 0.01$ between *PLC*ε$^{+/+}$ and *PLC*ε$^{\Delta X/\Delta X}$ mice.

and frequency of the phospho-Smad1/5/8-positive cells were similar to those in the *PLC*ε$^{+/+}$ counterparts (Fig. 5B and C). In striking contrast to the *PLC*ε$^{+/+}$ pulmonary valves, the *PLC*ε$^{\Delta X/\Delta X}$ pulmonary valves exhibited an increase in the frequency of phospho-Smad1/5/8 positive cells on E14.5 (Fig. 5B and C). The aortic valves also showed similar phenomena (data not shown). We next investigated ErbB1 activation in the developing semilunar valves. While no apparent difference existed in the extent of ErbB1 activation in *PLC*ε$^{\Delta X/\Delta X}$ pulmonary and aortic valves on E14.5 (Fig. 5D and data not shown), a significant increase in the number of activated ErbB1-harboring cells where Smad1/5/8 was simultaneously activated was observed (Fig. 5D and E). This suggested that activated ErbB1 failed to suppress Smad1/5/8 activation in the absence of PLCε. Taking these data together, it was concluded PLCε may play an important role in ErbB1-mediated negative regulation of the Smad1/5/8 activation at a late stage of semilunar valve development, specifically on E14.5.

DISCUSSION

We have shown here that loss of the enzymatic function of PLCε results in congenital malformation of the semilunar valves, which causes a moderate to severe degree of regurgitation with a mild degree of stenosis. Phenotypes affecting the heart are unprecedented in mice deficient in any other classes of PLCs (9). The malformation apparently affects the semilunar valves but not the atrioventricular valves. Heart valve development consists of a number of complex processes. During mouse embryogenesis, premature hearts have a tubular structure consisting of endocardial and myocardial layers by E8.0; these layers are separated by an abundant extracellular matrix, cardiac jelly. After heart looping occurs at around E9.5, endocardial cells which reside in the atrioventricular canal and outflow tract undergo epithelium-to-mesenchyme transformation to form the atrioventricular and outflow tract cushions, respectively (13). The epithelium-to-mesenchyme transformation begins to abate by E12.5 (17), and a population of atrioventricular cushion cells subsequently develop into leaflets of the atrioventricular valves at the junction of the atria and ventricles. The outflow tract cushions fuse medially starting on E11.5 and, along with the assistance of neural crest-derived cells, separate the outflow tract into two distinct arteries, the aorta and pulmonary trunk (6). The interventricular foramen closes by E14.5 (27). Semilunar valves develop from the endocardial cushion cells at the distal ends of the proximal outflow tract segment through remodeling or cavitation of the cushion cells to form the definitive cup-shaped valvular leaflets along with their sinusal walls (28). *PLC*ε$^{\Delta X/\Delta X}$ mice did not show any discernible defect in the development of the atrioventricular valves and the aorticopulmonary and interventricular septations. Also, the appearance of the developing semilunar valves of *PLC*ε$^{\Delta X/\Delta X}$ mice remained normal through E15.5; thickening first appeared on E16.5 (Fig. 4D). These observations support a possible role of PLCε in remodeling the semilunar valves, particularly at the later stages of valvulogenesis, which is also consistent with our finding that *PLC*ε$^{\Delta X/\Delta X}$ mice showed aberrant activation of bone morphogenetic protein signaling specifically on the preceding day, E14.5 (Fig. 5B).

The remarkable resemblance of the semilunar valve pheno-

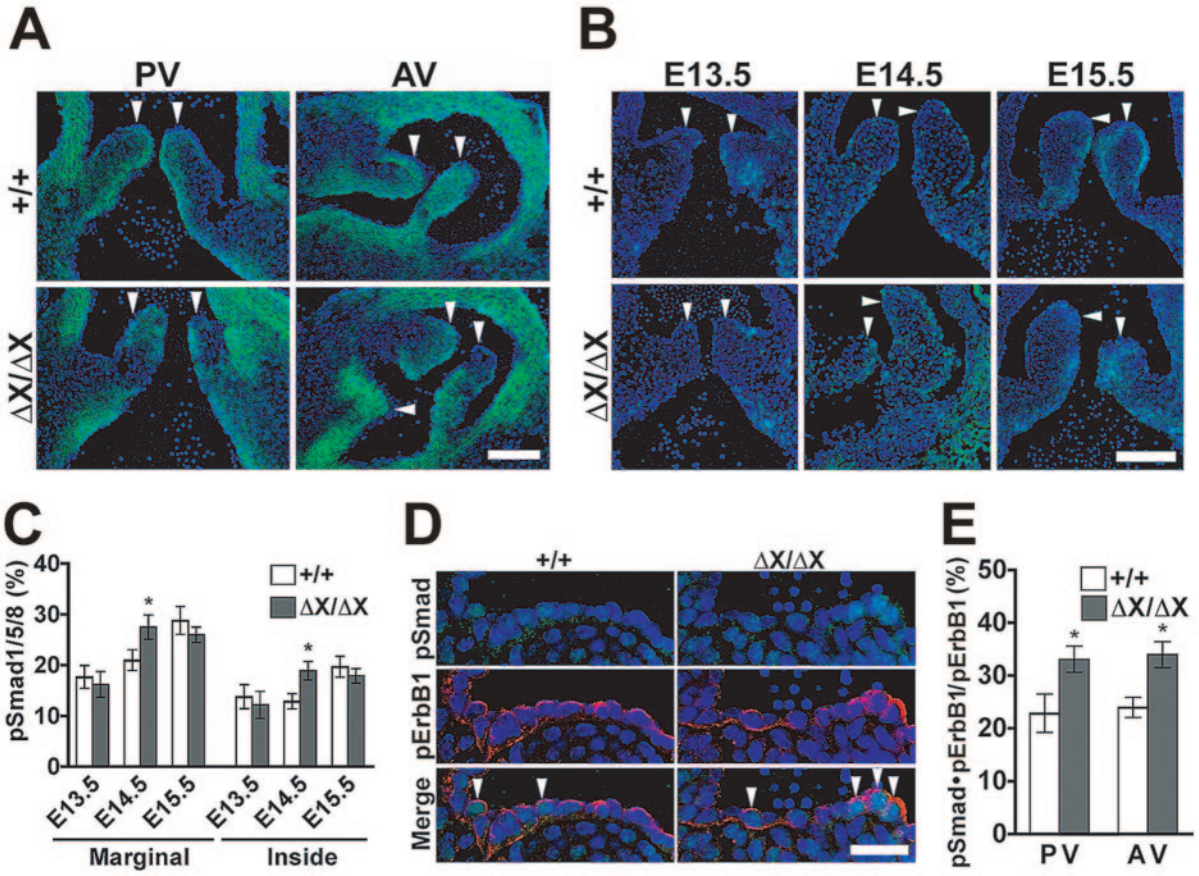

FIG. 5. PLCε expression and Smad1/5/8 activation in the developing semilunar valves. (A) Expression of PLCε in the pulmonary and aortic valves (PV and AV, respectively). The pulmonary valves of E14.5 *PLC*$\varepsilon^{+/+}$ (+/+) and *PLC*$\varepsilon^{\Delta X/\Delta X}$ (ΔX/ΔX) littermate embryos were stained with anti-PLCε antibody (green) along with DAPI (blue). White arrowheads indicate the valve leaflets. Scale bars, 50 μm. (B) Activation of Smad1/5/8 in the developing pulmonary valves. The pulmonary valves of *PLC*$\varepsilon^{+/+}$ and *PLC*$\varepsilon^{\Delta X/\Delta X}$ littermate embryos were subjected to immunostaining with anti-phospho-Smad1/5/8 antibody (green). Nuclei were stained with DAPI (blue). White arrowheads indicate the valve leaflets. Scale bars, 50 μm. (C) Quantification of phospho-Smad1/5/8-positive cells. The frequency of the phospho-Smad1/5/8-positive cells in the marginal or inside region of the pulmonary valves is shown. At least eight embryos of each genotype were analyzed. (D) Aberrant activation of Smad1/5/8 in the developing *PLC*$\varepsilon^{\Delta X/\Delta X}$ semilunar valves. The pulmonary valves of littermate embryos of E14.5 were stained with anti-phospho-Smad1/5/8 (green) and anti-phospho-ErbB1 (red) antibodies along with DAPI (blue). White arrowheads indicate the cells doubly positive for phospho-ErbB1 and phospho-Smad1/5/8. Scale bar, 20 μm. (E) Quantification of phospho-ErbB1- and phospho-Smad1/5/8-double-positive cells in the pulmonary and aortic valves. The ratio of the phospho-Smad1/5/8- and phospho-ErbB1-double-positive cells to phospho-ErbB1-positive cells was calculated. At least six embryos from each genotype were analyzed. *, $P < 0.05$ between *PLC*$\varepsilon^{+/+}$ and *PLC*$\varepsilon^{\Delta X/\Delta X}$ mice.

type of *PLC*$\varepsilon^{\Delta X/\Delta X}$ mice to that of mice deficient in HB-EGF or its receptor suggests a role of the Ras/Rap1-PLCε pathway downstream of HB-EGF signaling. Like *HB-EGF*$^{-/-}$ mice (12), *PLC*$\varepsilon^{\Delta X/\Delta X}$ mice show aberrant activation of receptor-regulated Smad, Smad1/5/8, in the developing semilunar valve cells (Fig. 5B). Activation of receptor-regulated Smad is known to induce hyperplasia of the cardiac valves (10). The distribution of HB-EGF expression in the developing heart valves is confined to the margins of the valve leaflets (11, 12), where we have observed the aberrant Smad1/5/8 activation (Fig. 5B) as well as the strong expression of PLCε (Fig. 5A). These observations taken together suggest that PLCε mediates the HB-EGF–ErbB1-dependent negative regulation of Smad1/5/8 activation. Although the antagonistic effect of ErbB1 signaling on Smad activity has hitherto been thought to be mediated by the Ras-Raf-extracellular signal-regulated kinase pathway from the studies with cultured cell lines COS-1 and R-1B/L17 (16), we failed to observe any increase in extracellular signal-regulated kinase activity in the developing semilunar valves of *PLC*$\varepsilon^{\Delta X/\Delta X}$ mouse heart (data not shown).

In *HB-EGF*$^{-/-}$ and *ErbB1*$^{-/-}$ mice, cardiac dilation is much more severe than that of *PLC*$\varepsilon^{\Delta X/\Delta X}$ mice, leading to death during the embryonic or early perinatal period (4, 11, 12). These mice exhibit a marked thickening of the both semilunar and atrioventricular valves. In contrast, *Egfr*$^{wa2/wa2}$ mice, expressing an ErbB1 mutant (*wa-2*) with a residual (10 to 20% of normal) intrinsic tyrosine kinase activity, have a long life span, and only the semilunar valves show thickening (4, 12) as observed in *PLC*$\varepsilon^{\Delta X/\Delta X}$ mice. This difference in the nature of the affected valves may be ascribed to differential sensitivities in the strength of HB-EGF–ErbB1 signaling or to differential hemodynamic loads (26) during development between the semilunar and atrioventricular valves.

The relationship between PLCε and human heart diseases is

not clear. The *PLC*ε gene is located on human chromosome 10q23, where a candidate gene for a familial dilated cardiomyopathy affecting one family has been mapped (3). However, this familial dilated cardiomyopathy is reported to involve mitral valve prolapse in addition to a pure dilated cardiomyopathy (3), which seems to be quite different from the phenotype of *PLC*$\varepsilon^{\Delta X/\Delta X}$ mice. It is well known that valvular dysfunction is a common type of human congenital heart disease (2). More than half of patients with semilunar valvular disease ≤65 years of age have congenital bicuspid valves (19). On the other hand, semilunar valvular disease maintaining the three-leaved (tricuspid) structure has been thought to be mostly acquired, with either rheumatic or age-dependent degenerative origin (19). However, a number of such cases are thought to be congenital. Our present results imply that some of these cases, especially those showing thickened semilunar valve leaflets that do not affect the atrioventricular valves, may have an etiological connection with a defect of the *PLC*ε gene. In addition, thickening and/or the uneven formation of the valve leaflets in *PLC*$\varepsilon^{\Delta X/\Delta X}$ mice may aggravate the age-dependent deformation process such as the commissural fusion (Fig. 4B), which may give an acquired bicuspid-like appearance. Existing mouse models of aortic valve deformities caused by gene disruptions exhibit an absolutely short life span (4, 11, 12). Therefore, it has been difficult to conduct detailed analyses of this phenotype. Since *PLC*$\varepsilon^{\Delta X/\Delta X}$ mice exhibit a long life span of at least 2 years, we believe that these mice will serve as a good animal model for deeper understanding of the pathophysiology of congenital valve malformations, such as the effects of exercise, stress, aging, or infectious diseases such as rheumatic fever.

ACKNOWLEDGMENTS

This work was supported by Grants-in-Aid for Scientific Research in Priority Areas (12215098) and for Scientific Research (15390093, 16790187, and 15570117) and by a 21st Century COE Program from the Ministry of Education, Science, Sports and Culture of Japan.

We thank Atsu Aiba and Tadashi Murase for helpful discussion and Seiichi Otake for excellent technical assistance.

REFERENCES

1. **Bai, Y., H. Edamatsu, S. Maeda, H. Saito, N. Suzuki, T. Satoh, and T. Kataoka.** 2004. Crucial role of phospholipase Cε in chemical carcinogen-induced skin tumor development. Cancer Res. **64:**8808–8810.
2. **Bartram, U., M. M. Bartelings, H. H. Kramer, and A. C. Gittenberger-de Groot.** 2001. Congenital polyvalvular disease: a review. Pediatr. Cardiol. **22:**93–101.
3. **Bowles, K. R., R. Gajarski, P. Porter, V. Goytia, L. Bachinski, R. Roberts, R. Pignatelli, and J. A. Towbin.** 1996. Gene mapping of familial autosomal dominant dilated cardiomyopathy to chromosome 10q21-23. J. Clin. Investig. **98:**1355–1360.
4. **Chen, B., R. T. Bronson, L. D. Klaman, T. G. Hampton, J. F. Wang, P. J. Green, T. Magnuson, P. S. Douglas, J. P. Morgan, and B. G. Neel.** 2000. Mice mutant for Egfr and Shp2 have defective cardiac semilunar valvulogenesis. Nat. Genet. **24:**296–299.
5. **Cheng, H. F., M. J. Jiang, C. L. Chen, S. M. Liu, L. P. Wong, J. W. Lomasney, and K. King.** 1995. Cloning and identification of amino acid residues of human phospholipase Cδ1 essential for catalysis. J. Biol. Chem. **270:**5495–5505.
6. **Délot, E. C.** 2003. Control of endocardial cushion and cardiac valve maturation by BMP signaling pathways. Mol. Genet. Metab. **80:**27–35.
7. **Ellis, M. V., U S, and M. Katan.** 1995. Mutations within a highly conserved sequence present in the X region of phosphoinositide-specific phospholipase C-δ1. Biochem. J. **307:**69–75.
8. **Essen, L. O., O. Perisic, R. Cheung, M. Katan, and R. L. Williams.** 1996. Crystal structure of a mammalian phosphoinositide-specific phospholipase Cδ. Nature **380:**595–602.
9. **Fukami, K.** 2002. Structure, regulation, and function of phospholipase C isozymes. J. Biochem. **131:**293–299.
10. **Galvin, K. M., M. J. Donovan, C. A. Lynch, R. I. Meyer, R. J. Paul, J. N. Lorenz, V. Fairchild-Huntress, K. L. Dixon, J. H. Dunmore, M. A. Gimbrone, Jr., D. Falb, and D. Huszar.** 2000. A role for Smad6 in development and homeostasis of the cardiovascular system. Nat. Genet. **24:**171–174.
11. **Iwamoto, R., S. Yamazaki, M. Asakura, S. Takashima, H. Hasuwa, K. Miyado, S. Adachi, M. Kitakaze, K. Hashimoto, G. Raab, D. Nanda, S. Higashiyama, M. Hori, M. Klagsbrun, and E. Mekada.** 2003. Heparin-binding EGF-like growth factor and ErbB signaling is essential for heart function. Proc. Natl. Acad. Sci. USA **100:**3221–3226.
12. **Jackson, L. F., T. H. Qiu, S. W. Sunnarborg, A. Chang, C. Zhang, C. Patterson, and D. C. Lee.** 2003. Defective valvulogenesis in HB-EGF and TACE-null mice is associated with aberrant BMP signaling. EMBO J. **22:**2704–2716.
13. **Jiang, X., D. H. Rowitch, P. Soriano, A. P. McMahon, and H. M. Sucov.** 2000. Fate of the mammalian cardiac neural crest. Development **127:**1607–1616.
14. **Jin, T.-G., T. Satoh, Y. Liao, C. Song, X. Gao, K. Kariya, C. D. Hu, and T. Kataoka.** 2001. Role of the CDC25 homology domain of phospholipase Cε in amplification of Rap1-dependent signaling. J. Biol. Chem. **276:**30301–30307.
15. **Kelley, G. G., S. E. Reks, J. M. Ondrako, and A. V. Smrcka.** 2001. Phospholipase Cε: a novel Ras effector. EMBO J. **20:**743–754.
16. **Kretzschmar, M., J. Doody, and J. Massague.** 1997. Opposing BMP and EGF signalling pathways converge on the TGFβ family mediator Smad1. Nature **389:**618–622.
17. **Lakkis, M. M., and J. A. Epstein.** 1998. Neurofibromin modulation of ras activity is required for normal endocardial-mesenchymal transformation in the developing heart. Development **125:**4359–4367.
18. **Lopez, I., E. C. Mak, J. Ding, H. E. Hamm, and J. W. Lomasney.** 2001. A novel bifunctional phospholipase C that is regulated by Gα12 and stimulates the Ras/mitogen-activated protein kinase pathway. J. Biol. Chem. **276:**2758–2765.
19. **Roberts, W. C.** 1992. Morphologic aspects of cardiac valve dysfunction. Am. Heart J. **123:**1610–1632.
20. **Schmidt, M., S. Evellin, P. A. Weernink, F. von Dorp, H. Rehmann, J. W. Lomasney, and K. H. Jakobs.** 2001. A new phospholipase-C-calcium signaling pathway mediated by cyclic AMP and a Rap GTPase. Nat. Cell Biol. **3:**1020–1024.
21. **Schroeder, J. A., L. F. Jackson, D. C. Lee, and T. D. Camenisch.** 2003. Form and function of developing heart valves: coordination by extracellular matrix and growth factor signaling. J. Mol. Med. **81:**392–403.
22. **Shibatohge, M., K. Kariya, Y. Liao, C. D. Hu, Y. Watari, M. Goshima, F. Shima, and T. Kataoka.** 1998. Identification of PLC210, a *Caenorhabditis elegans* phospholipase C, as a putative effector of Ras. J. Biol. Chem. **273:**6218–6222.
23. **Song, C., C. D. Hu, M. Masago, K. Kariya, Y. Yamawaki-Kataoka, M. Shibatohge, D. Wu, T. Satoh, and T. Kataoka.** 2001. Regulation of a novel human phospholipase C, PLCε, through membrane targeting by Ras. J. Biol. Chem. **276:**2752–2757.
24. **Song, C., T. Satoh, H. Edamatsu, D. Wu, M. Tadano, X. Gao, and T. Kataoka.** 2002. Differential roles of Ras and Rap1 in growth factor-dependent activation of phospholipase Cε. Oncogene **21:**8105–8113.
25. **Toker, A.** 1998. The synthesis and cellular roles of phosphatidylinositol 4,5-bisphosphate. Curr. Opin. Cell Biol. **10:**254–261.
26. **Topper, J. N., and M. A. Gimbrone, Jr.** 1999. Blood flow and vascular gene expression: fluid shear stress as a modulator of endothelial phenotype. Mol. Med. Today **5:**40–46.
27. **Webb, S., N. A. Brown, and R. H. Anderson.** 1998. Formation of the atrioventricular septal structures in the normal mouse. Circ. Res. **82:**645–656.
28. **Webb, S., S. R. Qayyum, R. H. Anderson, W. H. Lamers, and M. K. Richardson.** 2003. Septation and separation within the outflow tract of the developing heart. J. Anat. **202:**327–342.
29. **Wing, M. R., D. Houston, G. G. Kelley, C. J. Der, D. P. Siderovski, and T. K. Harden.** 2001. Activation of phospholipase C-ε by heterotrimeric G protein βγ-subunits. J. Biol. Chem. **276:**48257–48261.
30. **Wing, M. R., J. T. Snyder, J. Sondek, and T. K. Harden.** 2003. Direct activation of phospholipase C-ε by Rho. J. Biol. Chem. **278:**41253–41258.
31. **Wu, D., M. Tadano, H. Edamatsu, M. Masago-Toda, Y. Yamawaki-Kataoka, T. Terashima, A. Mizoguchi, Y. Minami, T. Satoh, and T. Kataoka.** 2003. Neuronal lineage-specific induction of phospholipase Cε expression in the developing mouse brain. Eur. J. Neurosci. **17:**1571–1580.